

Microstructural design of materials for aerostatic bearings

T.H. Panzera^{a,*}, J.C. Rubio^a, C.R. Bowen^{b,1}, P.J. Walker^{c,2}

^a *Department of Mechanical Engineering, Federal University of Minas Gerais, Av. Antônio Carlos 6627, Campus Pampulha, 31.270.901 Belo Horizonte, MG, Brazil*

^b *Materials Research Centre, Department of Mechanical Engineering, University of Bath, Bath BA2 7AY, UK*

^c *Department of Architecture and Civil Engineering, University of Bath, Bath BA2 7AY, UK*

Received 19 April 2006; received in revised form 14 June 2007; accepted 6 August 2007

Available online 5 September 2007

Abstract

The aim of this work is to investigate the development of a high strength porous cementitious composite manufactured via cold-pressed compaction for use as the restrictor in aerostatic bearings for high precision applications since they provide a number of advantages over conventional orifice restrictors. The selection of suitable materials and microstructural design of composites phases is essential to the development of material for optimum stiffness, strength, porosity and permeability. A variety of high purity (99.98% SiO₂) silica particle types was mixed with ordinary Portland cement to produce the composite mixtures. A full factorial design (2²4¹) was carried out to study the effects of silica properties (size and geometry) and uniaxial pressures (10 MPa and 30 MPa) on mechanical properties and microstructure of the ceramic composites. The cementitious composite manufactured using small silica particles, non-spherical shape and low level of compaction pressure exhibited the most appropriate properties for the stated application of porous bearings.
© 2007 Elsevier Ltd. All rights reserved.

Keywords: Porous bearing; Cementitious composite; Full factorial design

1. Introduction

Common applications of air bearings include profile projection equipment employing air bearing slides, rotary measuring tables and machine tool lead screw measuring heads [1]. Aerostatic bearings are able to provide a small variation of properties with temperature, high damping, high operational speeds, limited wear and capacity to support radial, axial and combined loadings [2]. Aerostatic bearings operate on the principle of supporting a load on a thin film of high pressure air which flows continuously out of the bearing and into the atmosphere. Since air has

a very low viscosity, bearings gaps need to be small and are typically of the order of 1–10 μm [3]. Air bearings are typically classed as orifice or porous media types. In orifice bearings the pressurized air arrives at the bearing surface through a small number of precisely sized machined holes. The use of a porous material as the bearing surface to provide a large number of minute restrictors, uniformly distributed over the entire bearing surface, can potentially create a highly uniform pressure distribution, and thus the highest load capacity and stiffness. Typically, aerostatic air bearings provide improved accuracy of up to two orders of magnitude better than that of conventional rolling element bearings [4].

Despite its many advantages, the availability of porous material with predictable fluid flow characteristics has continued to hamper the widespread application of porous aerostatic bearings. While much of the work immediately after the last review by Kwan [5] concentrated on the dynamic theories of such bearings, the most recent interests have been centred on material development. Most

* Corresponding author. Tel.: +55 (32) 33792603; fax: +55 (32) 33717070.

E-mail addresses: tuliopanzera@hotmail.com (T.H. Panzera), juan@ufmg.br (J.C. Rubio), c.r.bowen@bath.ac.uk (C.R. Bowen), P.Walker@bath.ac.uk (P.J. Walker).

¹ Fax: +44 (0) 1225 386928.

² Fax: +44 (0) 01225 386691.

examples of porous aerostatic bearings published so far have been based on metallic or graphite materials [6], because of their lower cost and also an ease of machining. The use of porous ceramics with improved hardness in such applications would, however, eliminate the problems of pore smearing, which is one of the main causes of poor permeability control associated with other ductile materials.

According to Kwan and Corbett [4], the material requirements for porous aerostatic circular thrust bearings with a simple single-layered porous pad working at 5–15 μm design gaps should exhibit: porosity level between 20% and 35%, permeability coefficient between 3.1×10^{-15} and $8.4 \times 10^{-14} \text{ m}^2$ and mechanical strength around 35 MPa. Amongst the most important characteristics, the restrictor should have a uniform open pore structure, with permeability coefficients which are consistent and repeatable from batch to batch. Pores should be uniform, both in terms of size and spatial distribution. The bearing should be lightweight, especially for highly dynamic applications with high accelerations. It should have a high modulus of elasticity to minimise deflection, and be strong enough to sustain the working pressure.

In these respects, the aim of this work is to investigate the development of a cementitious composite as a potential bearing material. In the last decades progressive improvements have been occurring in cementitious materials. Techniques for production of ultra-high strength cementitious composite include the use of fine materials [7–10], chemical admixtures [9,11], very low water–cementitious material ratio [7,9–14], compaction by pressure [9,10,12,13,15–18], high temperature curing [8–10,17,18] and autoclave curing [8].

The present work concerns a design of experiment (DOE) approach based on factorial design for the consideration of interactions of composite properties and processing parameters. The DOE approach can be divided into a full factorial design and a fractional factorial design. The full factorial design has the advantages that all of the main effects and interactions can be considered. A full factorial design (2^{24}) and the analysis of variance (ANOVA) technique will be applied to identify the significance of the composition and manufacturing factors on the responses. The statistical software “Minitab 14” was used to analyse the results. The factors and responses were chosen in order to provide a better understanding regarding the material microstructure and the desired effective properties, such as, high stiffness, high compressive strength, high permeability coefficient and high porosity level.

2. Experimental work

Based on the following studies, [7,9,11,15,19] the chosen factors for the manufacture of the composites were: “silica particle size”, “silica particle shape” and “uniaxial compaction pressure”. The silica particle size was divided in four size levels, each one with a mono size particle distribution: 500 μm , 250 μm , 125 μm and 44 μm . The silica parti-

cle shape was divided into two levels, namely spherical and non-spherical. The compaction pressure was divided into two levels: 10 MPa and 30 MPa. The water/cement (w/c) mass ratio (0.20) and silica/cement (s/c) ratio (0.67) were maintained constant in all experimental treatments. The materials responses to be considered, bulk density, modulus of elasticity (via compression testing), compressive strength, apparent porosity, average pore size and permeability, were considered to be relevant to aerostatic bearing applications. The experiment might be replicated, which means that the experimental plan should be manufactured two or more times. The minimum of two replicates used in this work ensured validity of the estimate of experimental error and provides a basis for inference in analysing the experiments. In addition to replication, the experimental treatments were also randomised in terms of the order providing protection against variables that are unknown to the experiment but may impact the response [20]. Thus, 16 experimental treatments (C1 up to C16) were designed for the present experiment (Table 1), which combined a variety of processing factors (aggregate particle size, shape and pressing pressure). The statistical analysis carried out in this work provides a relevant contribution not only in precision engineering but also in the cement and concrete technology. The experimental factors and the respective levels chosen in this work will now be described.

2.1. Matrix phase: cement

The Portland cement used for all mixes was Brazilian CP V ARI PLUS (ASTM Type III). Table 2 describes the chemical analysis of the cement.

2.2. Dispersive phase: silica

In order to investigate the size and geometry effects of the silica particles on the mechanical properties of the

Table 1
Experimental treatments for composite manufacture

E.T.	Factors/levels		
	Size (μm)	Geometry	Pressure (MPa)
<i>Full factorial design – 2²⁴</i>			
C1	500	Spherical	30
C2	500	Spherical	10
C3	500	Non-spherical	30
C4	500	Non-spherical	10
C5	250	Spherical	30
C6	250	Spherical	10
C7	250	Non-spherical	30
C8	250	Non-spherical	10
C9	125	Spherical	30
C10	125	Spherical	10
C11	125	Non-spherical	30
C12	125	Non-spherical	10
C13	44	Spherical	30
C14	44	Spherical	10
C15	44	Non-spherical	30
C16	44	Non-spherical	10

Table 2
Chemical analysis of cement

Chemical composition	(%)
CO ₂ (%)	1.13
SO ₃ (%)	2.85
SiO ₂ (%)	19.45
Al ₂ O ₃ (%)	4.75
Fe ₂ O ₃ (%)	3.12
CaO (%)	64.14
MgO (%)	0.8
K ₂ O (%)	0.66
Loss in ignition (1000 °C)	3.31
Free lime	0.67
Physical properties	
Specific surface (Blaine)	472.9 m ² /kg

cementitious composite, two types of silica particles were chosen: spherical and non-spherical. High purity (99.98%) silica particles (SiO₂) from Minas Gerais State in Brazil were selected. With regard to particle size, they have been classified through a standard mineral sieving process in mono size distribution in order to achieve a consistent distribution of pore sizes (Table 3). The addition of fine silica particle in cementitious composites in order to obtain high strengths has been studied by many researchers [7,9,11].

2.3. Silica and cement ratio (*s/c*)

Li and Ding [21] have studied the effects of the amount of Portland cement in terms of chemical and physical aspects. The silica/cement ratio of 0.67 was observed to provide the highest compressive strength. This dosage was adopted as a constant factor in all experimental treatments in this work.

2.4. Water and cement ratio (*w/c*)

The reduction of *w/c* ratio causes (i) a decrease of the total porosity of the hardened paste, (ii) an acceleration of cement hydration during its initial period and (iii) the formation of hydration products with a smaller amount of bound water and with a substantially higher specific binding capacity [13,17]. Higher strengths at very low *w/c* ratios are attributed to direct formation of the cubic C₃AH₆ phase on the original sites of the cement minerals. The small amount of additional hydration is sufficient to “glue” the dense clinker particles together and modify the stress field at regions of interparticle contact [22].

Table 3
Sieving processing for particle sizes

Particle size (μm)	Oversize sieve (US Tyler)	Undersize sieve (US Tyler)
<i>Monosize particle distribution</i>		
500	35	40
250	60	70
125	120	140
44	325	400

According to Toossi, Iran [10], results demonstrate that a reduced *w/c* ratio from 0.30 to 0.20 does not significantly reduce the total porosity compared to that of higher *w/c* ratios. Zhang and Gjorv [11] stated that although the total porosity decreased with decreasing *w/c* ratio, the pore size distribution was not very different for *w/c* ratios of 0.25 and 0.20. It has been shown that [23] the lower the *w/c* ratio the lower the permeability of the cement paste at a specific level of hydration. In addition, the permeability does not vary significantly for *w/c* ratios in the range of 0.20–0.30.

Therefore, the *w/c* ratio used in the present cementitious composite was 0.20. This amount of *w/c* ratio not only produces the highest range of strengths, but also ensures that all the water in the mixture will be chemically bound when producing calcium silicate hydrate (C–S–H), thus preventing the formation of large voids [9].

2.5. Compaction pressure

According to Cannillo et al., Bonneau et al. [16,22], the application of pressure can have three effects: (i) the reduction of entrapped air, (ii) excess water removal and (iii) chemical shrinkage compensation. The reduction of porosity due to exertion of pressure can be the main cause for the increased strength [9,10]. Roy et al. [18] observed that hot-pressed (150 °C) cement specimens did not show a significant difference in the pore size distribution from those compacted by vibration and the effect of the increasing of pressing pressure on pore size reduction was small.

Although the hot-pressing process provides high compressive strengths [17], conventional cold press compaction has been chosen in this work. Based on the studies of Bajza [15] and Cheeseman et al. [19], two levels of compaction pressure were considered relevant: 10 MPa and 30 MPa. The samples were manipulated in a room with temperature and humidity controlled at 25 °C and 65%, respectively. Hand mixing of Portland cement, silica particles and water was performed based on British Standard (BS NS 8000). The samples were compacted for 1 min and then sealed in plastic bags to avoid the loss of water. Plastic tubes inside a steel die were used to manufacture the pressed samples with 0.0276 m of diameter. The samples were cured for 28 days in a cylindrical box at room temperature. Using a precision saw, the samples were cut to ensure the same height of 0.0453 m.

3. Experimental results and discussion

The experimental data obtained in this investigation, including bulk density, modulus of elasticity, compressive strength, apparent porosity, average pore size and permeability are summarized in Tables 4 and 5. Table 4 details the results for the replicate 1 and Table 5 includes the results for the replicate 2. The average pore size has not been statistically analysed since results for only replicate 1 are available. The standard deviations and the means

Table 4
Experimental results for replicate 1

E.T.	Bulk density (kg/m ³)	Modulus of elasticity (GPa)	Compressive strength (MPa)	Apparent porosity (%)	Oxygen permeability (×10 ⁻¹⁶ m ²)	Average pore size (μm)
C1	2376.00	26.63	86.75	7.31	0.82	0.0124
C2	2366.00	43.57	94.94	8.40	0.89	0.0091
C3	2356.00	45.03	83.12	7.91	0.97	0.0092
C4	2331.00	51.62	97.36	8.92	0.69	0.0143
C5	2318.00	37.62	75.47	7.99	1.03	0.0090
C6	2321.00	50.78	91.77	9.93	0.79	0.0151
C7	2347.00	40.73	79.76	8.11	0.75	0.0090
C8	2285.00	45.08	87.78	10.13	1.44	0.0156
C9	2242.00	44.42	75.50	14.48	1.86	0.0183
C10	2199.00	51.47	87.49	15.61	5.68	0.0210
C11	2239.00	39.42	59.37	11.23	1.17	0.0095
C12	2202.00	43.27	75.06	13.62	11.51	0.0200
C13	2147.00	40.33	76.66	16.03	6.16	0.0108
C14	2105.00	46.88	71.97	17.55	16.37	0.0120
C15	2068.00	45.28	77.07	17.03	25.98	0.0244
C16	2020.00	41.83	71.41	19.77	64.54	0.0115

Table 5
Experimental results for replicate 2

E.T.	Bulk density (kg/m ³)	Modulus of elasticity (GPa)	Compressive strength (MPa)	Apparent porosity (%)	Oxygen permeability (×10 ⁻¹⁶ m ²)	Average pore size (μm)
C1	2378.00	35.70	88.18	6.23	0.77	–
C2	2332.00	49.18	85.66	7.85	0.98	–
C3	2353.00	46.05	76.43	8.32	0.98	–
C4	2323.00	55.60	106.12	9.74	0.77	–
C5	2338.00	36.73	60.21	8.82	0.96	–
C6	2328.00	52.87	86.13	10.38	0.92	–
C7	2313.00	36.37	68.11	9.53	0.89	–
C8	2280.00	36.77	73.71	10.50	0.82	–
C9	2209.00	31.85	56.33	13.48	2.02	–
C10	2166.00	41.52	67.83	15.45	6.37	–
C11	2235.00	41.52	66.08	10.14	1.50	–
C12	2176.00	34.80	66.56	14.62	11.27	–
C13	2159.00	35.65	59.88	15.89	5.16	–
C14	2115.00	39.80	66.96	18.53	14.82	–
C15	2096.00	40.93	77.59	17.97	20.01	–
C16	2036.00	38.10	66.87	20.34	101.36	–

of the measurements were not reported due to the statistical methodology is able to identify the location and the dispersion of the data by the replicates and the randomized order. The replicates can estimate the true error variance and also detect the effect significance.

The analysis of variance was performed by the statistical software “*Minitab 14*”. The *P*-values (Table 6) indicate which of the effects in the system are statistically significant, based on examination of the experimental data from replicate 1 and replicate 2. If the *P*-value is less than or

Table 6
Analyses of variance (ANOVA), *P*-values ($\alpha \leq 0.05$)

Source	Bulk density	Modulus of elasticity	Compressive strength	Apparent porosity	Oxygen permeability
Size	0.000	0.497	0.000	0.000	0.000
Geometry	0.000	0.508	0.988	0.246	0.000
Pressure	0.000	0.001	0.010	0.000	0.000
Size * geometry	0.000	0.017	0.675	0.000	0.000
Size * pressure	0.314	0.127	0.151	0.164	0.000
Geometry * pressure	0.175	0.010	0.719	0.248	0.008
Size * geometry * pressure	0.458	0.950	0.199	0.269	0.004
<i>R</i> ² (%)	99.02	74.60	77.38	98.99	94.80
Standard deviation	0.015	4.548	7.919	0.579	6.604

equal to 0.05 it is possible to conclude that the effect is significant. An α -level of 0.05 is the level of significance which implies that there is 95% of probability of the effect being significant. The results will be presented via ‘main effect’ and ‘interaction’ plots. These graphic plots cannot be considered a typical ‘scatter’ plots, but serve to illustrate the statistical analysis and provide the variation on the significant effects.

(a) *Main effects plots*: The ‘main effects’ plot is most useful when you have several factors such as particle size, particle shape and pressing pressure that influence the composite property. These plots are used to compare the changes in the mean level to examine which of the processing factors influence the response (e.g. bulk density) the most. A ‘main effect’ is present when different levels of a factor affect the response differently. Fig. 1 shows some examples of main effect plots where particle size, particle shape and pressing pressure significantly influence the bulk density. This type of plot is used to examine the mean value for each factor, compare the mean value for several factors and compare the relative strength of the effects across factors.

(b) *Interaction effects*: In addition to a ‘main effect’, there may also be ‘interaction effect’. An interaction is present when the change in the mean response of the composite (e.g. bulk density) from a low to high level of a factor (e.g. particle size) depends on the level of a second factor (e.g. particle shape) [20]. Interactions plots are used to visualize the interaction effect of two or more factors (e.g. size and geometry; size and pressure; geometry and pressure; size, geometry and pressure) on the response and to compare the relative strength of the effects. Fig. 2 shows an interaction plot whereby composites manufactured using the small silica particle size exhibit the lowest bulk density, but the variation of bulk density with particle size also depends on the particle shape.

3.1. Bulk density

In terms of bulk density, Table 6 shows that the P -values for all three main effects of particle size, particle geometry and pressure are zero and obviously less than 0.05. Therefore, there is strong evidence of a significant effect of bulk density on particle size, geometry and pressing pressure. Fig. 1 shows the main effects of size (Fig. 1a), geometry (Fig. 1b) and pressure (Fig. 1c) which demonstrates that when you change from a low to high particle “size” and pressing “pressure”, the bulk density increases. When particle “geometry” changes from the spherical to non-spherical the bulk density is observed to decrease. The bulk density data for all the samples vary from 2020 kg/m³ to 2380 kg/m³.

The “size and geometry” interaction is also a significant factor with P -value (0.000) less than 0.05. The small 44 μ m particles provide the smallest bulk density and it is possible to observe in the interaction plot in Fig. 2 that there is also a decrease in density when changing from 44 μ m spherical

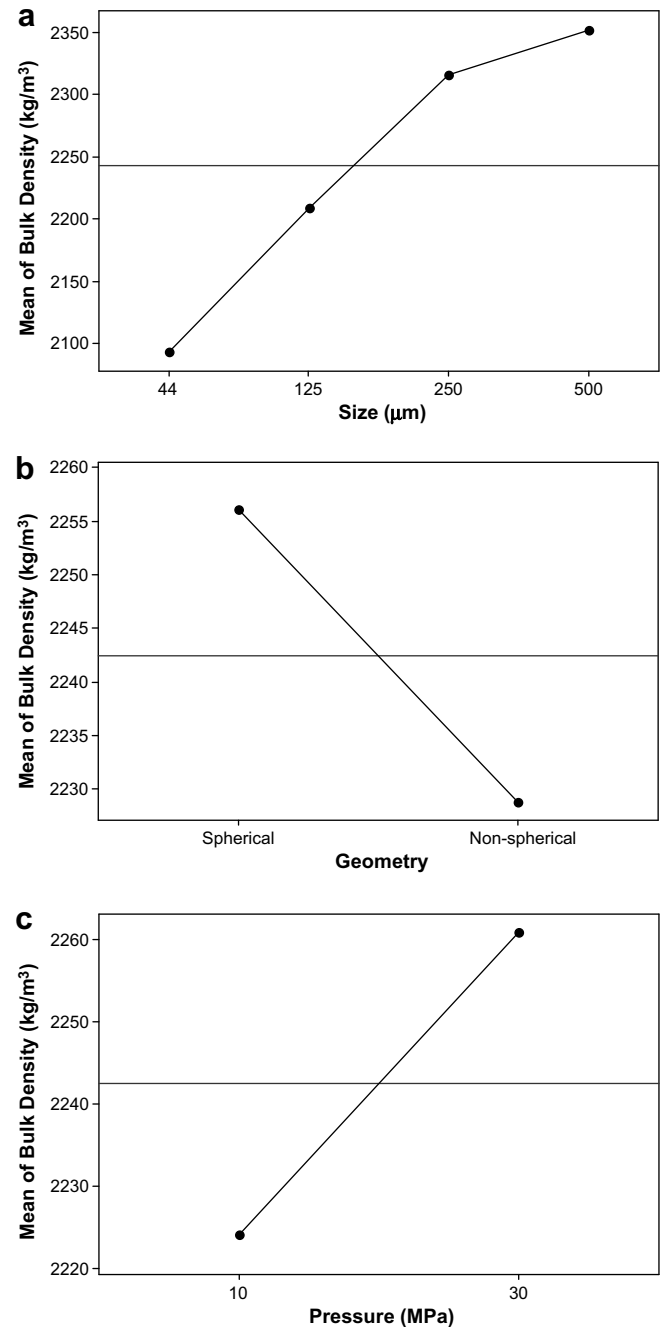


Fig. 1. Main effects plot for bulk density: (a) size, (b) geometry and (c) pressure.

to 44 μ m non-spherical shaped particles. The particle size factors of 500 μ m and 250 μ m also show a decrease in the bulk density when using non-spherical geometry particles, although for a particle size of 125 μ m only a small variation of bulk density between spherical and non-spherical particles is observed.

The R^2 value represents the proportion of variation in the response data explained by the terms in the model. The R^2 value given in Table 4 (99.02%) shows that the model postulated for the bulk density measurements fits the data well.

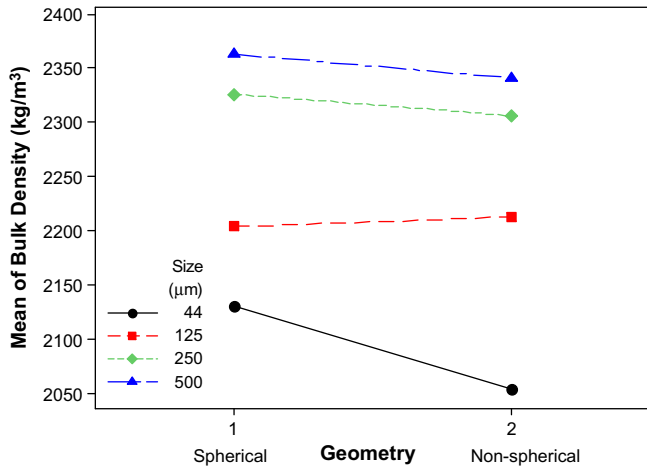


Fig. 2. Interaction plot for bulk density.

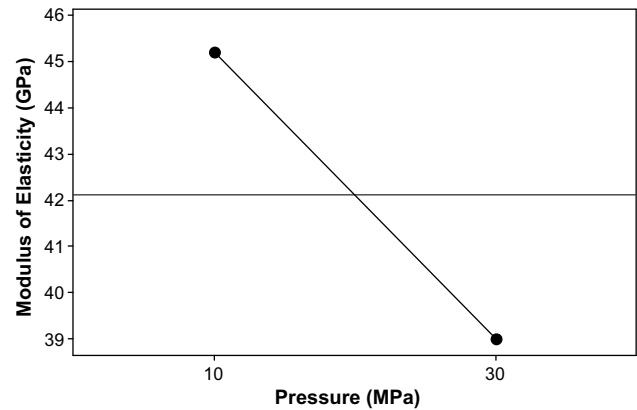


Fig. 3. Main effects plot for modulus of elasticity.

The material for porous bearings should be lightweight [4], especially for highly dynamic applications with high accelerations, which means low bulk densities. The highest bulk density is reached when the experimental treatment is set as large particle size, spherical shape and high pressure. However, the lowest bulk density is reached when the experimental treatment is set as small particle size, non-spherical shape and low level of pressure, which corresponds to the experimental treatment C16 in Table 1.

3.2. Modulus of elasticity

The modulus of elasticity has been determined from the use of strain gauges in a compression test (British Standard, BS 1881/121). The data results are shown in Tables 4 and 5, which demonstrate that the modulus of elasticity data varies from 26.63 GPa to 55.60 GPa. For the modulus of elasticity, there are three significant effects when $\alpha \leq 0.05$ (Table 1). These significant effects include one main effect, “pressure” (0.001) and two interactions effects, “size and geometry” (0.017) and “size and pressure” (0.010).

The main effect plot in Fig. 3 shows that when we change from a 10 MPa to 30 MPa pressing pressure, the modulus of elasticity decreases by 13%. This behaviour is thought to be related with the hydration process of the cement paste [16,22]. It is possible that the water content was not sufficient to hydrate the paste in the high pressure level due to water being dragged to the sample surfaces during pressing at 30 MPa.

From the interaction plot “size and geometry” of Fig. 4 we can observe that the largest (500 μm) and the smallest (44 μm) particles provide the highest modulus when the silica particles are non-spherical in geometry. The largest particles present a variation of 20% when changing from spherical to non-spherical particles. The particles 250 μm and 125 μm provide the highest modulus of elasticity when using silica particles with spherical geometry.

The interaction factor of “geometry and pressure” for the modulus of elasticity has a significant effect with P-

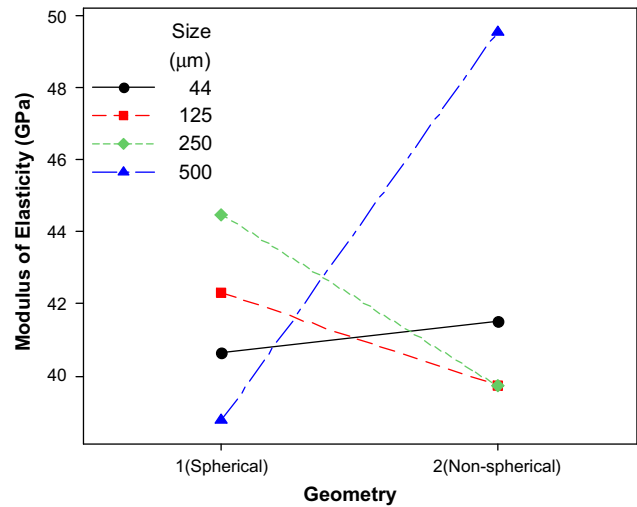


Fig. 4. Interaction plot (size and geometry) for modulus of elasticity.

value of 0.010 (Table 6). According to the interaction plot (Fig. 5), we can observe that spherical and non-spherical particle sizes provide a high modulus of elasticity when the low level of pressure (10 MPa) is used. It is also possible

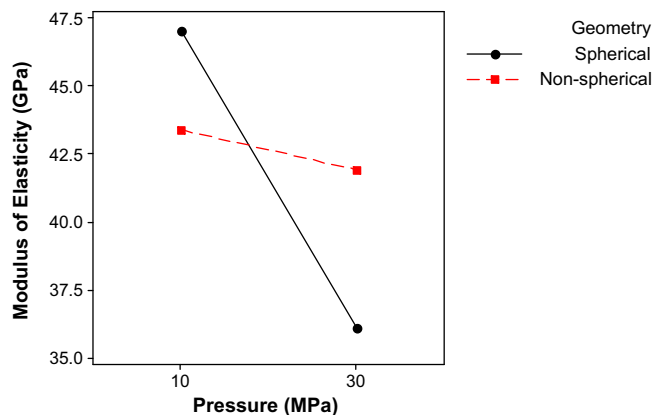


Fig. 5. Interaction plot (geometry and pressure) for modulus of elasticity.

to observe from the plot that the spherical particles provide a higher stiffness than non-spherical particles in the low level of pressure.

The high stiffness desired for porous bearing materials [4] should be achieved when the experimental treatment is set as large non-spherical particles at low pressure, see C4 in Table 1.

3.3. Compressive strength

The compressive strength was carried out based on the recommendations of British Standard (BS EN 12390). A test set consisted of five cylindrical test specimens. Since there were 16 experimental treatments and two replicates, 160 compression tests were carried out. For each test specimen, the concrete was taken at random from a different experimental treatment, distributed approximately uniformly over the production period to be investigated. The test was measured at 270 days. The compressive strength data varied from 56.33 MPa to 106.12 MPa (Tables 4 and 5).

The *P*-values of 0.000 and 0.010 for main effects of “size” and “pressure”, respectively, are less than 0.05 (Table 6), thus, there is evidence of a significant effect of particle size and pressure on compressive strength. The main effects plot for compressive strength (Fig. 6) shows

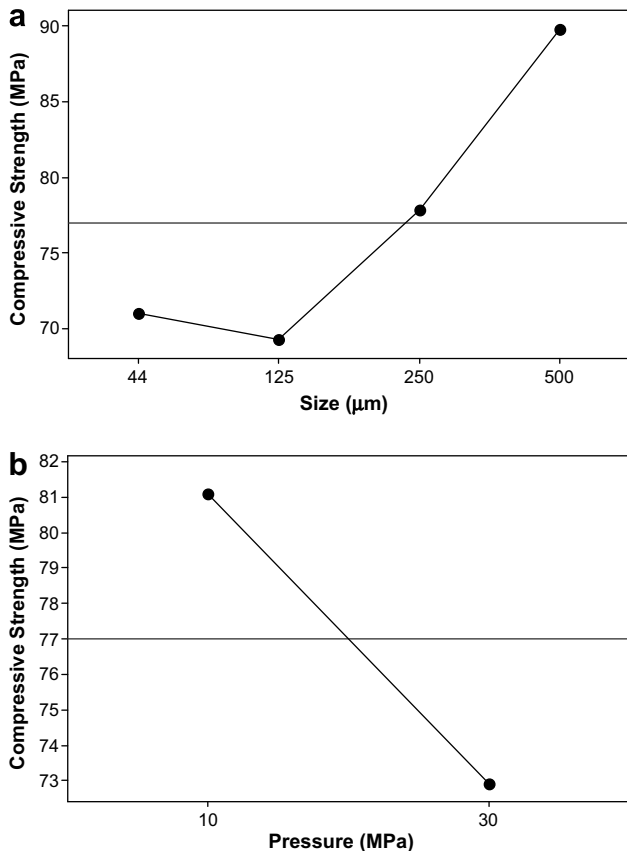


Fig. 6. Main effects for compressive strength: (a) size and (b) pressure.

that when you change from a low to high particle size, the compressive strength increases (Fig. 6a). In addition, when you change from the 10 MPa to 30 MPa level of pressure, the compressive strength decreases (Fig. 6b). According to [13] the compressive strength of hardened cement pastes is generally a power function of the amount of binding hydration products developed in them. The amount of water is possibly the main responsible for the decreasing the strength in the high level of pressure. According to Sadrekarimi [9] the higher the bulk density the greater the strength of the paste and lower the permeability since there are fewer and smaller voids. In this work, while the highest compressive strength is observed when using a 10 MPa pressing pressure, the highest bulk density is obtained when using a 30 MPa pressure.

The material requirements in terms of high strength [4] should be achieved when the composite is set as large spherical or non-spherical silica particles at low pressures (see experimental treatments C2 and C4 in Table 1).

3.4. Apparent porosity

The apparent porosity has been carried out based on the recommendations of British Standard (BS EN ISO 10545). The data results are presented in Tables 4 and 5. The porosity data varied from 6.23% to 20.34% (volume %). Table 6 shows the significant main factors for apparent porosity being “size”, “pressure” and the interaction factor “size and geometry”, both with the *P*-values of 0.000. The R^2 is 98.99% indicating the model postulated for the apparent porosity measurements fits the data very well.

According to Jambor [14], there are two distinct stages in the development of pore structure in cement composites. The first stage is determined by the composition of the mixture and by its compaction degree. The second stage is highly influenced by the hydration process, such as the volume increase of hydration products in the composites. The main effects plot for apparent porosity (Fig. 7) shows that when you change from the small to large particle size (Fig. 7a), and low to high pressure (Fig. 7b) the apparent porosity decreases. This indicates that large particles and high pressure provide lower apparent porosity, in accordance with Jambor [14]. This indicates that the compressive strength is not only correlated to the apparent porosity, but also with the binding capacity of hydration products.

Fig. 8 shows the interaction plot between “size and geometry” for apparent porosity. We can observe that, apart from particles of size 125 μm, spherical particles provide lower porosities than the non-spherical geometry.

The apparent porosity values required for porous bearings application should be between 20% and 35% [4]. The highest apparent porosities should be achieved when the cementitious composite is manufactured from small silica particles, non-spherical particles and low pressure (composite C16 in Table 1).

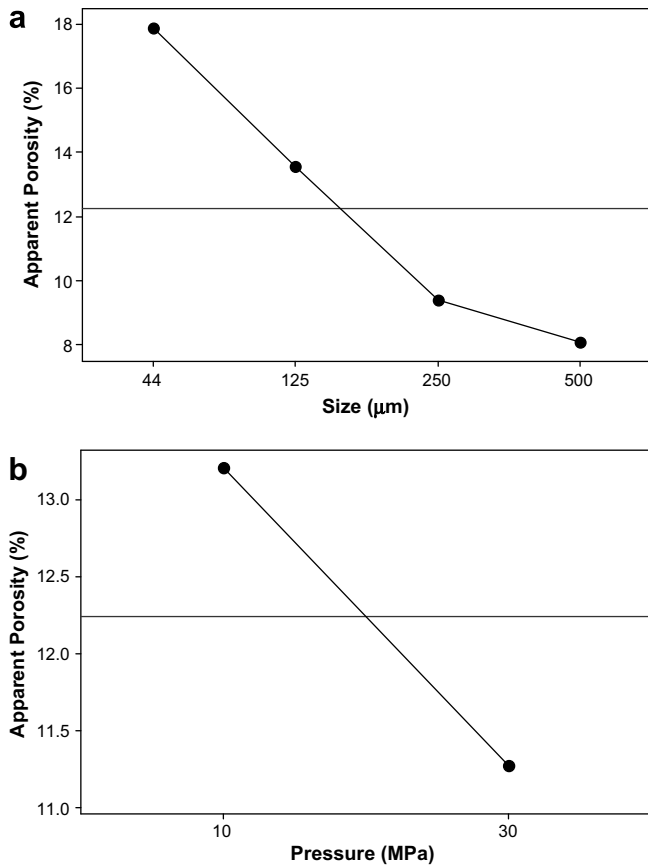


Fig. 7. Main effects plot for apparent porosity.

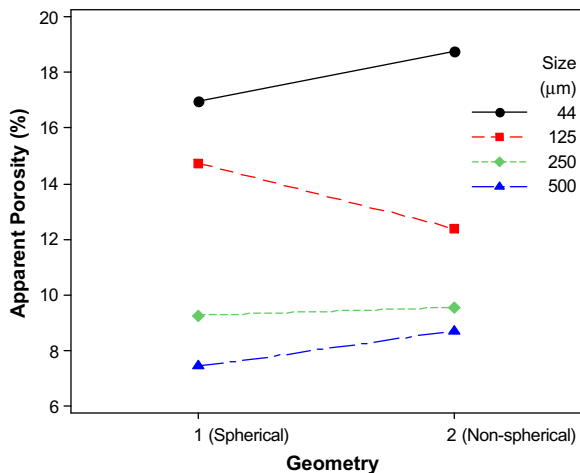


Fig. 8. Interaction plot for apparent porosity.

3.5. Oxygen permeability

Gas permeability testing was carried out in the University of Sheffield using an oxygen gas permeameter. The experimental procedure and further details about the test can be obtained from [24]. The permeability data results varied from 7.7×10^{-17} and $101.36 \times 10^{-16} \text{ m}^2$ and are presented in Tables 4 and 5.

The P -values for all three main effects in Table 4 are zero which is less than 0.05, which means there is an evidence of a significant effect of size, geometry and pressure on composite oxygen permeability. The R^2 is 94.80% indicating the model postulated for the oxygen permeability measurements fits the data well. As the interaction effect of size, geometry and pressure is also significant, only the interaction plot is analysed. It is possible to observe in Fig. 9 that the effects are in accordance with the apparent porosity results (Figs. 7 and 8), since the use of large particle sizes, spherical geometry and high pressure give the lowest permeability and lowest porosity results for the composites.

The possible reason for the reduced oxygen permeability in composites with large silica particles may be explained as follows. The amount of water used in the composites is low (water to cement ratio = 0.20) and the amount of water is not sufficient to fully hydrate all the cement grains. Those composites which are able to retain the most water are likely to be those with higher amount of hydrated cement phases and consequently higher density, strength and lower apparent porosity and oxygen permeability. The specific surface area is lower for the largest silica particles. As a result, a thicker film of water around the large particles may provide a better hydrating process, as well as the lowest oxygen permeability and the highest strength.

According to Kwan [5], the permeability coefficient required for porous bearings application should range from 3.1×10^{-15} to $8.4 \times 10^{-14} \text{ m}^2$. The oxygen permeability of the composites studied varied from 7.7×10^{-17} to $10.14 \times 10^{-15} \text{ m}^2$, indicating that the composites C14, C15 and C16 (Table 2) have the permeability requirements to be applied as porous bearings.

3.6. Average pore size

When designing a porous material, it is important to control not only the porosity and pore morphology, but also the pore spatial positioning if mechanical properties, such as fracture strength, are to be optimised [16]. The main parameters of pore structure which determine the strengths of cement composites are: total porosity, pore size distribution, pore morphology between the hydration products and between the cement matrix and aggregate, homogeneity of the composite, presence of structure flaws and macro pores acting as centres for formation of the failure cracks [14].

Mercury intrusion porosimetry tests were conducted using a *Micromeritics Porosimeter* (series v2.0). The samples were cut as a cube dimension. The samples were dried in an oven at 80 °C for 24 h. The average pore sizes were determined for only the replicate 1, thus the statistical analysis could not be performed. According to Table 4, the average pore sizes vary from 0.0090 μm to 0.0244 μm. Based on the results of average pore sizes the use of high pressure (30 MPa) provides a smaller average pore sizes compared to low pressures. The factors particle size and geometry did not demonstrate any significant effect.

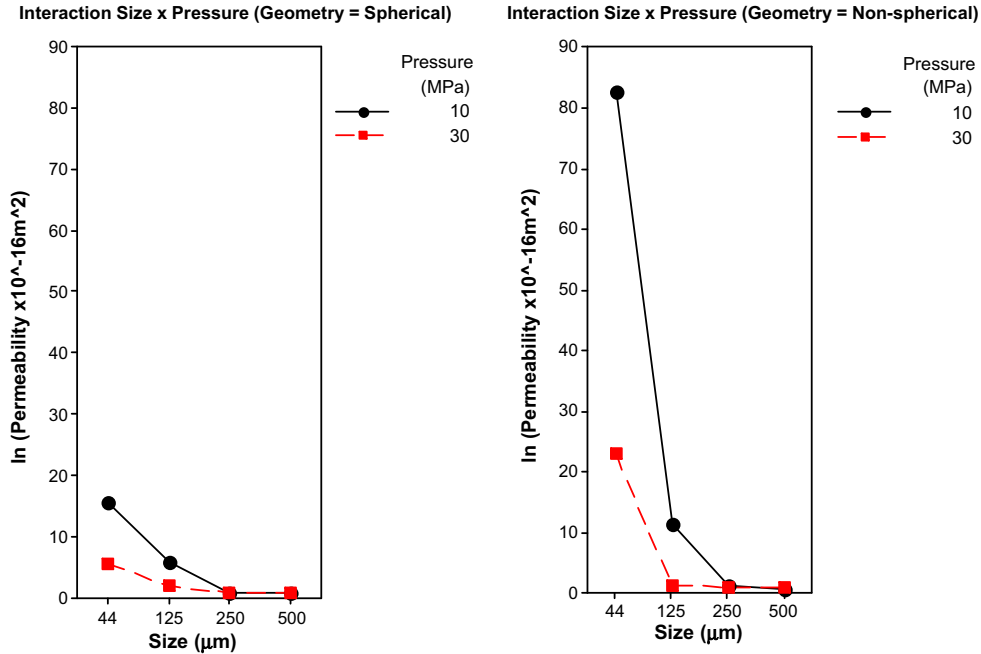


Fig. 9. Interaction effect plot for $\ln(\text{permeability})$, size, geometry and pressure.

All cementitious composites exhibited a similar behaviour in terms of pore size distribution. Two different pore sizes were observed in the composites: micropores in a range of 0.002–1 μm and the macropores in a range of 50–120 μm . Figs. 10 and 11 show two types of cementitious composites, C1 and C13, respectively. Composite 1 is manufactured using large particles (500 μm), spherical geometry, and high pressure (30 MPa). Composite 13 is manufactured from small particles (44 μm), spherical geometry and high pressure (30 MPa). It is possible to observe from Figs. 10 and 11 that the micro pores are predominant on the distribution of pore sizes showing a visible peak. An amount of macro pores is also presented with a small peak in a range of 50–120 μm . The backscatter SEM images observed from Figs. 12a and 13a indicate that micro pores are present in the cement paste and the macro pores are present at the interface zone between the silica particles and the cementitious matrix.

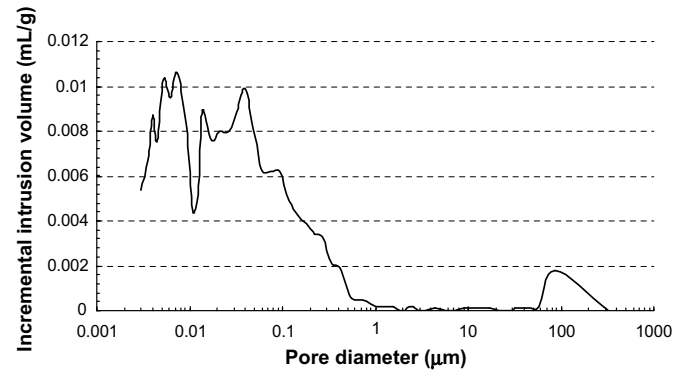


Fig. 11. Pore size distribution for composite 13.

Despite the presence of two types of pore sizes, it was possible to obtain a microstructure with a high concentration of micro pores, which means that the use of mono silica particles to reach a uniform pore size distribution was achieved.

3.7. Microstructure

Backscatter-mode scanning electron microscopy (SEM) was used for examination of the cementitious materials investigated in this work. Differences in backscatter coefficients primarily reflect differences in chemical composition among the different features present. Chemical components of high electron density have high backscatter coefficients, and appear bright in the backscattered images. Conversely, components of lower electron density, such as most cement hydration products, have lower backscatter coefficients and appear less bright [25].

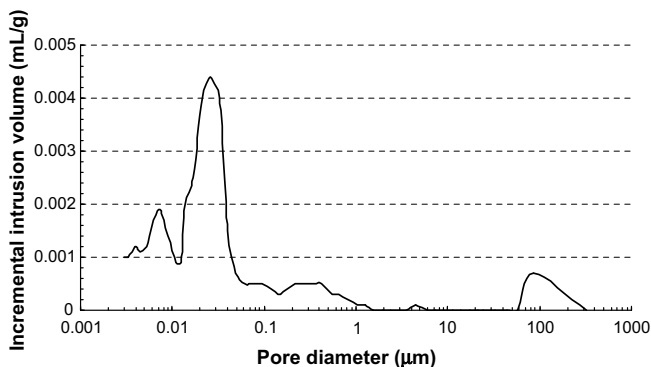


Fig. 10. Pore size distribution for composite 1.

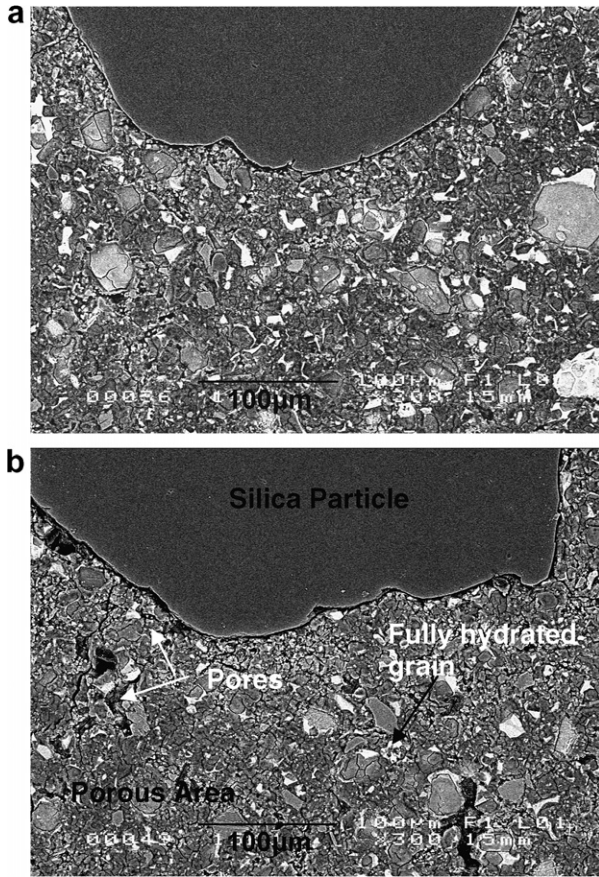


Fig. 12. Backscatter electron imaging at 300× of magnification: (a) C1 (0.500 mm, spherical with 30 MPa) and (b) C2 (0.500 mm, spherical with 10 MPa).

The hydration products found in most hardened Portland cement pastes primarily consist of C–S–H gel and calcium hydroxide, accompanied by smaller amounts of ettringite and monosulfate [25]. These hydration products are intermingled with pore spaces.

Fig. 12 illustrates composites C1 and C2 in backscatter-mode SEM with 300× of magnification. The composites have large silica particles (0.500 mm) with spherical geometry but they were compacted with 30 MPa (C1) and 10 MPa (C2) of pressure, respectively. The large dark areas in the Fig. 12a and b are the silica particles. The bright areas, which indicate the unhydrated components, are more evident in Fig. 12a than those in Fig. 12b. The removal of the excess of water in the high compaction pressure provides an unhydrated condition, as also observed by Canillo et al. [16] and Bonneau et al. [22]. The small dark areas observed in Fig. 12b are the large pores often located near the silica particles. Despite the unhydrated phase being denser than the hydrated phase, the presence of more unhydrated components can affect the bonding condition in the cement paste. According to the experimental results obtained in this work, the high level of pressure (Fig. 12a) provides high bulk density, low apparent porosity, low permeability, along with low modulus of elasticity and low compressive strength.

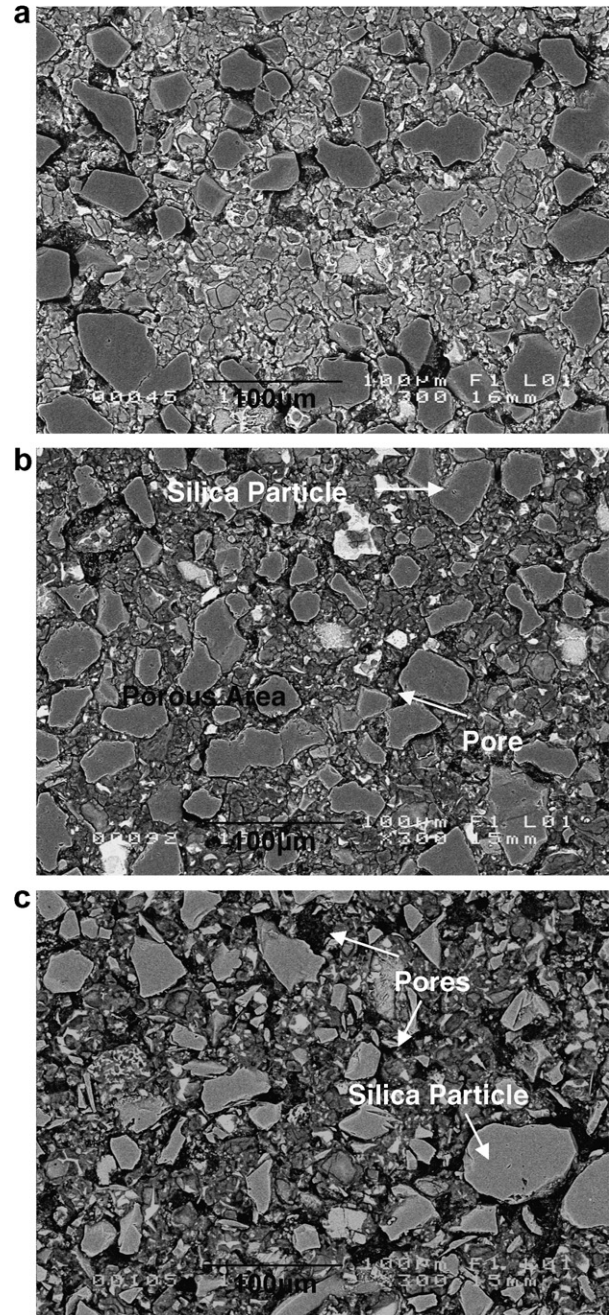


Fig. 13. Backscatter Electron Imaging at 300× of magnification: (a) C13 (0.044 mm, spherical with 30 MPa), (b) C14 (0.044 mm, spherical with 10 MPa) and (c) C16 (0.044 mm, non-spherical with 10 MPa).

Fig. 13a and b shows backscatter-mode SEM images of the composites C13 and C14, respectively. The composites contain the smallest silica particles (44 μm) with spherical geometry and are pressed at 30 MPa (Fig. 13a) and 10 MPa (Fig. 13b). The silica particles can be observed in Fig. 13 as large grey grains. The small silica particles provide a specific surface area per unit mass or volume larger than the large silica particles. In the same way, non-spherical particles provide a larger specific surface area than spherical particles. According to Neville [26], a larger

specific surface area of the silica particles lead to the absorption of a greater quantity of water, the effective water/cement ratio being thus reduced. Based on this phenomenon, it can be observed in Fig. 13a (30 MPa) that the amount of unhydrated area is larger than that obtained in Fig. 13b (10 MPa). A large amount of dark area is also observed in Fig. 13b, which indicates the presence of pores. Through the interaction plots for permeability (Fig. 9), it can be verified that the small silica particles produce a significant change from 10 MPa to 30 MPa pressure and particle geometry. Fig. 13c shows the microstructure of composite C16, made from small silica particles (44 μm) of non-spherical geometry at a low level of pressure (10 MPa). Comparing Fig. 13b and c, it is possible to observe that the composite C16 exhibits larger amount of pores than composite C14, which confirms using non-spherical silica particles reduce the hydration of the cementitious composites.

4. Conclusion

The design of experiments and full factorial analysis has been used to analyse and develop cementitious materials for aerostatic bearings with high strength, low bulk density, high permeability coefficient, and high porosity with open pore structure [4]. The main conclusions and effects will be now described:

- (i) The significant main factors obtained for the bulk density were particle size, particle geometry and compaction pressure. The interaction effect size and geometry is also a significant factor. Based on the stated application, the lowest bulk density is achieved when the main factors are set as, small particles (44 μm), non-spherical geometry and low pressure (10 MPa). The highest bulk density has been achieved when the significant main factors are set as, large particle size (500 μm), spherical particle shape and high pressure (30 MPa). This indicates that the optimisation of the particles packing can be enhanced with the pressing compaction and the correct selection of the particle size and geometry.
- (ii) The significant main factor obtained for modulus of elasticity was the compaction pressure. The significant interaction effects were “size and geometry” and “geometry and pressure”. The highest modulus of elasticity is achieved at the low level of pressure (10 MPa), which indicates that the water content was not sufficient to hydrate the paste in the high pressure level due to water being removed during pressing at 30 MPa. The same behaviour was also observed by Canillo et al. [16] and Bonneau et al. [22]. The interaction plots “size and geometry” and “geometry and pressure” indicated that the highest modulus of elasticity is reached when the composite contains large particles of non-spherical geometry and are pressed at a low level of pressure.

- (iii) The compressive strength demonstrated the particle size and the pressure as significant main factors. The highest compressive strength is achieved when the cementitious composites manufactured using: large particle size (500 μm) and low level of pressure (10 MPa). The removal of water in the high level of pressure should be the reason for the low strength at 30 MPa, despite it provides a large bulk density.
- (iv) The apparent porosity demonstrated particle size and the pressure as significant main factors. The largest porosity is required for porous bearings. The highest apparent porosity has been achieved when the composite is manufactured using small silica particles (44 μm) and low level of compaction pressure (10 MPa). The interaction effect size and geometry is also significant showing that the small particles provide a large apparent porosity for non-spherical geometry.
- (v) The three main factors (particle size, geometry and pressure) obtained a level of significance for the permeability coefficient. The highest permeability was achieved when the composite made from small particle size (44 μm), non-spherical geometry and low level of pressure (10 MPa), which means the presence of macro pores in the interface zone between the silica particle and the cement paste.
- (vi) According to the backscatter-mode SEM images and the pore size distribution obtained from MIP, the presence of two concentrations of pores was observed: the micro pores in a range of 0.002–1 μm and the macro pores in a range of 50–120 μm . The micro pores correspond to the most part of the distribution of pore sizes. The SEM images indicated that the micro pores are provided from the cement paste and the macro pores are provided from the interface zone between the silica particles and the cementitious matrix. The biggest average pore size is reached when the pressing compaction is set as 10 MPa.

Composites 14 and 16 which are made using small silica particles (44 μm) and low level of compaction pressure (10 MPa) optimise the properties and structure promising to be a significant material for the stated application of porous bearings. Other analyses including the interaction between responses were not presented in this paper to further optimise the properties for aerostatic bearing applications.

Acknowledgements

The authors wish to thank CAPES (Brazilian Agency for Postgraduate Programs), Holcim S/A (Portland cement), Moinhos Gerais Ltda (Silica particles), Dr. Cyril Lynsdale from the Department of Civil Engineering of the University of Sheffield, Mr. Paulo Borges (PhD student in the University of Sheffield) and Mr. Mike Lawrence (PhD student in the University of Bath).

References

- [1] Rubio JCC. Projeto, construção e avaliação de micro posicionadores para usinagem de ultraprecisão. PhD thesis. São Paulo: University of São Paulo; 2000.
- [2] Cheng K, Rowe WB. A selection strategy for the design of externally pressurized journal bearings. *Tribol Int* 1995;28(7):465–74.
- [3] Slocum A. Precision machine design. New Jersey: Prentice Hall; 1992.
- [4] Kwan YBP, Corbett J. Porous aerostatic bearings—an update review. *Wear* 1998;222(2):69–73.
- [5] Kwan YBP. Processing and fluid flow characteristics of hot isostatically pressed porous alumina for aerostatic bearing applications. PhD thesis. Cranfield: Cranfield Institute of Technology; 1996.
- [6] El-Aguizy T, Plante JS, Slocum AH, Vogan JD. Frictionless compression testing using load applying platens made from porous graphite aerostatic bearings. *Rev Sci Instrum* 2005;76(7):075108.
- [7] Ma J, Dietz J. Ultra high performance self compacting concrete. *Lacer*; 2002. p. 33–42.
- [8] Regourd M. Microstructure of high strength cement paste systems. In: Materials research society symposia proceedings, vol. 42; 1985. p. 3–17.
- [9] Sadrekarimi A. Development of a light weight reactive powder concrete. *J Adv Concrete Technol* 2004;2(3):409–17.
- [10] Toossi M, Iran T. Variation of concrete strength due to pressure exerted on fresh concrete. *Cement Concrete Res* 1980;10(6):845–52.
- [11] Zhang M, Gjorv OE. Effect of silica fume on pore structure and chloride diffusivity of low porosity cement pastes. *Cement Concrete Res* 1991;21(6):1006–14.
- [12] Beaudoin JJ, Feldman RF. High strength cement pastes. *Cement Concrete Res* 1985;15(1):105–16.
- [13] Jambor J. Influence of water–cement ratio on the structure and strength of hardened cement pastes. In: Proceedings of a conference held at university of sheffield, 8–9 April 1976; 1976. p. 175–88.
- [14] Jambor J. Pore structure and strength development of cement composites. *Cement Concrete Res* 1990;20(6):948–54.
- [15] Bajza A. Structure of compacted cement pastes. *Cement Concrete Res* 1983;13(2):239–45.
- [16] Cannillo V, Manfredini T, Montorsi M, Boccaccini AR. Use of numerical approaches to predict mechanical properties of brittle bodies containing controlled porosity. *J Mater Sci* 2004;39(13):4335–7.
- [17] Febrillet N, Fukuda H, Ito Y, Ishibashi K. Mechanical properties of ultra-high strength mortar made by using hot-press compaction. *Trans Jpn Concrete* 2002;23:45–56.
- [18] Roy DM, Gouda GR, Bobrowsky A. Very high strength cement pastes prepared by hot pressing and other high pressure techniques. *Cement Concrete Res* 1972;2:349–66.
- [19] Cheeseman CR, Asavapisit S, Knight J. Effect of uniaxial pressing ordinary Portland cement pastes containing metal hydroxides on porosity, density and leaching. *Cement Concrete Res* 1998;28(11):1639–53.
- [20] Jeff Wu CF, Hamada M. Experiments: planning, analysis, and parameter optimization. New York: John Wiley & Sons; 2000.
- [21] Li Z, Ding Z. Property improvement of Portland cement by incorporating with metakaolin and slag. *Cement Concrete Res* 2002;33(4):579–84.
- [22] Bonneau O, Poulin C, Dugat J, Richard P, Aitcin P. Reactive powder concretes: from theory to practice. *Concrete Int* 1996;18(4):47–9.
- [23] Powers TC, Copeland LE, Hayes JC, Mann HM. Permeability of Portland cement paste. *J Am Concrete Inst* 1954;26(3):285–97.
- [24] Cabrera JG, Lynsdale CJ. A new gas permeameter for measuring the permeability of mortar and concrete. *Mag Concrete Res* 1988;40(144):177–82.
- [25] Diamond S. The microstructure of cement paste and concrete – a visual primer. *Cement Concrete Compos* 2004;26(8):919–33.
- [26] Neville AM. Properties of concrete. New York: John Wiley & Sons; 1995.